universe

MDPI

Article

Diagram of High-Energy Nuclear Collisions †

Evgeny Andronov [1], Magdalena Kuich [2,*] and Marek Gazdzicki [3,4]

[1] Faculty of Physics, St. Petersburg State University, St. Petersburg 198504, Russia
[2] Faculty of Physics, University of Warsaw, 02-093 Warsaw, Poland
[3] Faculty of Physics, Geothe-University, 60438 Frankfurt am Main, Germany
[4] Faculty of Natural Sciences, Jan Kochanowski University, 25-406 Kielce, Poland
* Correspondence: mkuich@cern.ch
† This paper is based on work performed before 24 February 2022.

Abstract: Many new particles, mostly hadrons, are produced in high-energy collisions between atomic nuclei. The most popular models describing the hadron-production process are based on the creation, evolution and decay of resonances, strings or quark–gluon plasma. The validity of these models is under vivid discussion, and it seems that a common framework for this discussion is missing. Here, for the first time, we explicitly introduce the diagram of high-energy nuclear collisions, where domains of the dominance of different hadron-production processes in the space of laboratory-controlled parameters, the collision energy and nuclear-mass number of colliding nuclei are indicated. We argue that the recent experimental results suggest the location of boundaries between the domains, allowing for the first time to sketch an example diagram. Finally, we discuss the immediate implications for experimental measurements and model development following the proposed sketch of the diagram.

Keywords: high-energy collisions; strongly interacting matter; quark–gluon plasma; strings; resonances

PACS: 25.75.q; 25.75.Nq; 24.60.Ky

Citation: Andronov, E.; Kuich, M.; Gazdzicki, M. Diagram of High-Energy Nuclear Collisions. *Universe* **2023**, *9*, 106. https://doi.org/10.3390/universe9020106

Academic Editors: Carlos Pajares and Roman Pasechnik

Received: 7 January 2023
Revised: 3 February 2023
Accepted: 15 February 2023
Published: 18 February 2023

1. Introduction

One of the crucial issues of contemporary physics is understanding strong interactions—the interactions defining properties of atomic nuclei and collisions between them. Nuclear collisions at high energies lead to the production of many new particles, predominately strongly interacting hadrons. With the advent of the quark model of hadrons and the development of the commonly accepted theory of strong interactions, quantum chromodynamics (QCD) naturally led to expectations that matter at very high densities may exist in a state of quasi-free quarks and gluons, the quark–gluon plasma (QGP) [1]. There are numerous indications that QGP is created in heavy-ion collisions at high energies; for review, see Refs. [2–5].

The theoretical description of high-energy nuclear collision is not an easy task. This may be attributed to the difficulty of obtaining unique and quantitative predictions from QCD. In particular, even the formation of QGP in heavy-ion collisions is beyond the predictability of QCD. Consequently, the bulk properties of high-energy nuclear collisions are described by phenomenological models. Over time, three classes of them gained in popularity:

(i) One postulates that the final hadronic state emerges from the quark–gluon plasma's creation, evolution, and hadronisation [6]. A key input—the QGP equation of state—can be estimated using lattice-QCD calculations [7]. This process will be labelled as *QGP*;
(ii) One assumes hadrons originate from the formation, evolution and fragmentation of strings—the gluon fields between a pair of colour charges forming a narrow flux

tube [8]. Strings are typically oriented along the collision axis, and they have a continuous masses spectrum. Symmetries and experimental results are used to determine model parameters. This process will be labelled as *strings*;

(iii) One describes the production of final state hadrons by creation, evolution and decay of hadronic resonances [9]—excited states of stable hadrons. Resonances do not have a preferred elongation direction and have a discrete mass spectrum. Experimental results are used to determine model parameters. This hadron-production process will be labelled as *resonances*.

Do the processes reflect reality? If yes, what are the domains of their applicability? Answering these questions is directly related to understanding intriguing changes of hadron-production properties observed experimentally by varying collision energy and the mass number of colliding nuclei. This task goes hand in hand with selecting measurable quantities sensitive to a transition between the processes. In this paper, we focus the discussion on the ratio of positively charged kaons and pions measured at mid-rapidity, the K^+/π^+ ratio. This measure can be interpreted as a good approximation of the strange to non-strange quarks ratio. Due to mass and number differences between strange and non-strange particles (quarks and gluons or hadrons), the ratio is expected to be sensitive to the hadron-production process [10,11]—it is expected to be sensitive to a changeover between different processes. With the above and the availability of the rich experimental data, the choice of the K^+/π^+ ratio as the subject of this paper was most suitable.

For a quantitative comparison of the experimental results with model predictions, we selected PHSD [12,13] and SMASH [14,15] models. This is motivated by their important features. Both models give predictions in the full range collision energy and masses of the colliding nuclei covered by the experimental data. The SMASH model includes resonances and strings, whereas the PHSD model also includes QGP.

We review the experimental results and suggest the first answers to the questions asked in Section 2. Section 3 introduces the diagram of high-energy nuclear collisions, and we summarise our findings in a diagram sketch. Finally, we discuss the implications following the sketch for experimental measurements and developing models.

2. Guiding Ideas and Experimental Results

Heavy-ion collisions.

The richest experimental results on the collision energy dependence of hadron-production properties concern collisions between two heavy atomic nuclei, Pb+Pb and Au+Au collisions. Over the last 40 years, they were recorded in the hunt for QGP and the energy threshold of its creation—the *onset of deconfinement*. Many fixed-target and collider experiments in the US (Lawrence Berkeley Laboratory, LBL, and Brookhaven National Laboratory, BNL) and European (European Organization of Nuclear Research, CERN and Helmholtz Centre for Heavy Ion Research, GSI) laboratories have been conducting the measurements. The results are consistent with the onset of deconfinement being located at ($\sqrt{s_{NN}} \approx 8$ GeV) and the QGP being created at the early stage of heavy-ion collisions at higher collision energies (for review, see Refs. [2–5]). The most popular plot illustrating this assessment is presented in Figure 1 (left). It shows the collision energy dependence of the K^+/π^+ ratio in central heavy-ion collisions. The ratio shows the so-called *horn* structure. Following a fast rise, the ratio passes through a maximum in the CERN SPS energy range, at approximately 8 GeV, then decreases and settles to a plateau which continues up to the CERN LHC energies. Kaons are the lightest strange hadrons, and due to approximate isospin symmetry, the K^+ yield counts about half of the strange quarks produced in the collisions and contained in the reaction products [11]. Thus, Figure 1 (left) demonstrates that the fraction of strangeness carrying particles in the produced matter passes through a sharp maximum at the SPS energy range in central heavy-ion collisions; for a detailed explanation; see Ref. [4].

The standard modelling of heavy-ion collisions [6] includes the formation of high-density matter (be it QGP or hadronic matter) at the early stage of a collision, its expansion

and the decoupling of hadrons that freely stream to particle detectors. A statistical description of the early stage [11] led to predictions of the collision energy dependence of bulk hadron production properties. In particular, the horn structure was predicted as the signal of the onset of deconfinement. In the model, it reflects the decrease in the ratio of strange to non-strange degrees of freedom when deconfinement sets in. Experimental data are compared with calculations of the PHSD model [12,13] that incorporates the QGP creation at sufficiently high densities and chiral-symmetry restoration in the dense hadronic matter. The model catches the basic properties of the data; see Figure 1 (left). This further supports interpreting the horn maximum at $\sqrt{s_{NN}} \approx 8$ GeV as the beginning of the QGP creation. Moreover, the SMASH model [14,15], which does not include the QGP creation qualitatively, fails to reproduce the results; see Figure 1 (left). One should, however, note that there are significant uncertainties in modelling both production processes; see below for an example.

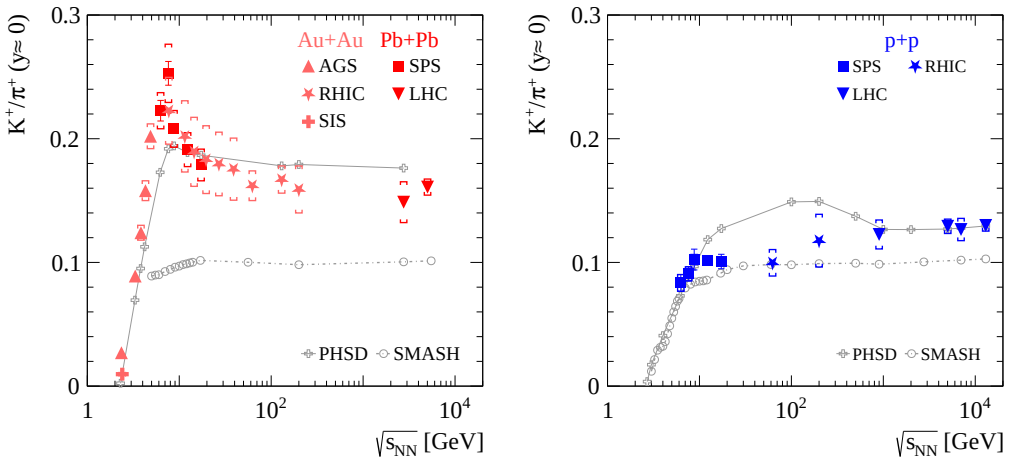

Figure 1. Collision energy dependence of the K^+/π^+ multiplicity ratio at mid-rapidity in central heavy-ion collisions (Pb+Pb [16–19] and Au+Au [20–26]) (**left**) and in inelastic p+p interactions [19,27–31] (**right**). Open cross points present the PHSD [12,13] predictions, while open circles—the SMASH [14,15] predictions. Lines connecting the points are plotted to guide the eye.

Proton–proton interactions.

Measurements of proton–proton interactions started long before the first experiments studying heavy-ion collisions. The primary goal of the study of p+p interactions was understanding strong interactions. With increasing collision energy, more and heavier hadrons have been produced. To understand the early results, the string model was invented [32]. The experimental results also contributed to the formulation of QCD—the nowadays commonly accepted theory of strong interactions. While there is no first-principles derivation of strings from QCD, some properties of a string can be derived from QCD.

Paradoxically, QCD demotivated studies of bulk properties of p+p interactions. This is because of difficulties in obtaining unique and quantitative predictions from QCD. Consequently, the world data on p+p interactions are not as rich as the corresponding results on heavy-ion collisions. The compiled data on the K^+/π^+ ratio at mid-rapidity in inelastic p+p interactions is shown in Figure 1 (right). Precise measurements are available at the CERN SPS and LHC energies. The p+p results still allow for important observations:

(i) At the SPS energies, the ratio in p+p interactions is about a factor of two lower than in heavy-ion collisions;
(ii) At $\sqrt{s_{NN}} \approx 8$ GeV, a *break* in the collision energy dependence of the ratio is observed in p+p interactions instead of the horn seen in heavy-ion collisions. For a more detailed analysis of the p+p break, see Ref. [33];
(iii) At the LHC energies, the p+p ratio is about 20% lower than the heavy-ion one.

The most popular modelling of proton–proton interactions at high energies includes strings' formation, evolution, and fragmentation. The widely used approaches are the Lund [34], EPOS [8] and Dual Parton [35,36] models. At low collision energies, the validity of the string approach breaks, and one replaces it with the creation of resonances and their decay; for a detailed explanation, see Ref. [15]. These two processes are implemented in the PHSD [12,13] and SMASH [14,15] models.

Their predictions for the collision energy dependence of the K^+/π^+ ratio in *p*+*p* interactions are shown in Figure 1 (right). Significant differences between them shed light on the uncertainty of the predictions. Taking into account this uncertainty, one concludes that the models reproduce the bulk properties of the data.

The effect of the changeover from resonances to strings (*onset of strings*) was studied in detail within the UrQMD model [37,38]. Within SMASH [14,15], the changeover causes a wiggle in the collision energy dependence of the K^+/π^+ ratio, which can be seen in Figure 1 (right) by enlarging the plot. In PHSD [12,13], a sharp transition is located at $\sqrt{s_{NN}} \approx 2.6$ GeV—close to the threshold for kaon production—and thus its effect on the ratio is hard to observe.

The open question discussed in Ref. [33] is whether the break (ii) in the collision energy dependence of the experimental ratio at $\sqrt{s_{NN}} \approx 8$ GeV is due to the onset of strings or is related to the onset of deconfinement.

One notes the following regarding the similarity of the ratio in *p*+*p* and Pb+Pb collisions at LHC (iii). It was reported that relative strange hadron yields in *p*+*p* interactions at LHC smoothly increase with increasing charged-particle multiplicity and for high multiplicity interactions are close to those in Pb+Pb collisions [39]. Moreover, recent LHC data on the azimuthal angle distribution of charged particles in high multiplicity *p*+*p* interactions [40–42] show anisotropies up to the recently observed only in heavy-ion collisions and attributed to the hydrodynamical expansion of matter [43]. This suggests that QGP may also be produced in *p*+*p* interactions at the LHC energies, at least in collisions with sufficiently high hadron multiplicity.

Collisions of intermediate-mass nuclei.

The collision-energy dependence of hadron-production properties in collisions of intermediate-mass nuclei is the least established one. The only systematic measurements have been performed at the CERN SPS by NA61/SHINE [44].

They were motivated by a search for the critical point of strongly interacting matter and a need to establish the nuclear mass dependence of the horn structure [45]. The data on collisions of intermediate-mass nuclei are summarised in Figure 2. The results of K^+/π^+ ratio for central Pb+Pb/Au+Au and inelastic *p*+*p* are also plotted for comparison in a light colour. The main observations are:

(i) The ratio in Be+Be collisions is similar to the one in *p*+*p* interactions in the whole SPS energy range;
(ii) There is no horn structure in Ar+Sc collisions;
(iii) The ratio in Ar+Sc collisions at the top SPS energy is similar to the one in Pb+Pb collisions.

Figure 3 shows results on the K^+/π^+ ratio measured at $\sqrt{s_{NN}} \approx 7.7$ GeV (the left plot) and $\sqrt{s_{NN}} \approx 17$ GeV (the right plot) as a function of the mean number of nucleons that participated in inelastic interactions, the so-called number of wounded nucleons $\langle W \rangle$. Since,, at high collision energies, the ratio is weakly dependent on the collision energy, results from central Au+Au collisions at $\sqrt{s_{NN}} = 19.6$ GeV were also included in the plot.

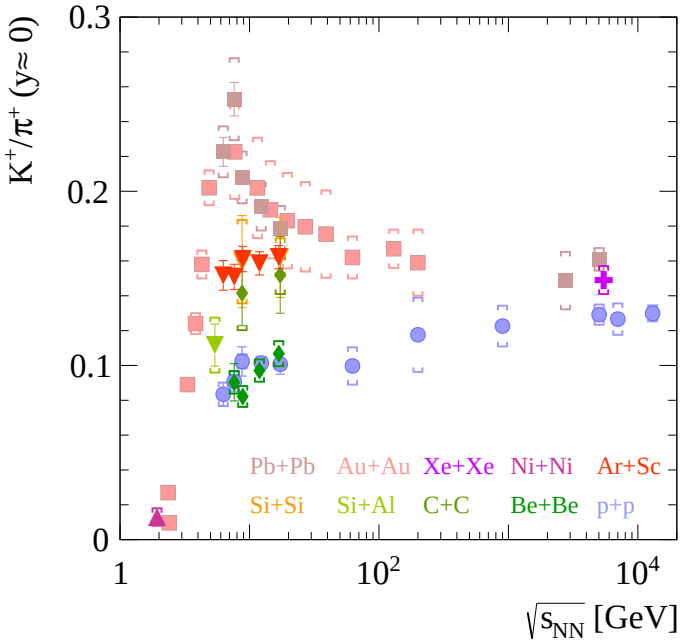

Figure 2. Status of experimental results on energy dependence of the K^+/π^+ ratio at mid-rapidity in high-energy nuclear collisions. In addition to the previously shown results on central heavy-ion collisions [16–26] and inelastic p+p [19,27–31] interactions, results on central Be+Be [46], C+C [47,48], Si+Al [49], Si+Si [47,48], Ar+Sc (preliminary) [50,51], Ni+Ni [52,53] and Xe+Xe [54] collisions are shown. Points presenting Pb+Pb/Au+Au and p+p are plotted in pale colours to emphasize intermediate-mass nuclei results.

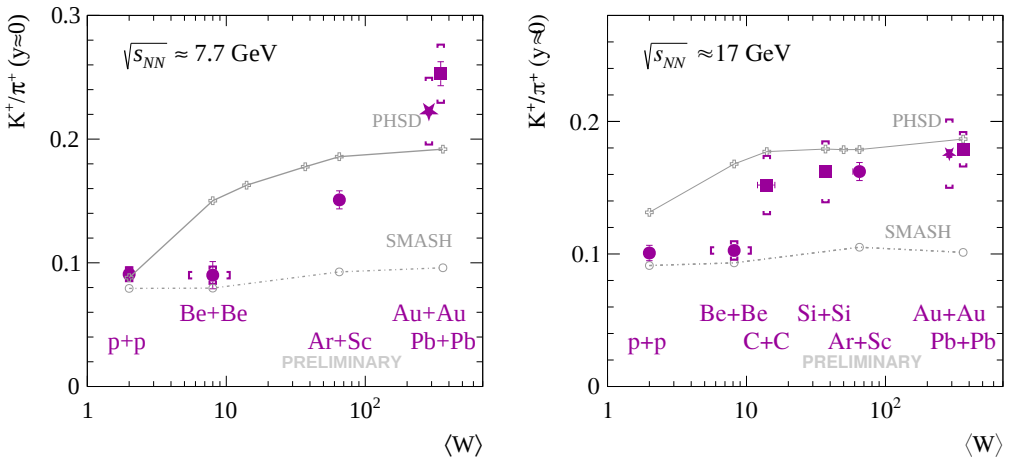

Figure 3. The K^+/π^+ ratio at mid-rapidity measured at $\sqrt{s_{NN}} \approx 7.7$ GeV (**left**) and $\sqrt{s_{NN}} \approx 17$ GeV (**right**) as a function of a mean number of wounded nucleons, $\langle W \rangle$, in inelastic p+p interactions [27] and central Be+Be [46], C+C [47], Si+Si [47], Ar+Sc (preliminary) [50,51], Au+Au [22], Pb+Pb [16,17] collisions. Experimental results were compared with the PHSD [12,13] (open crosses) and SMASH [14,15] (open circles) predictions. Lines are plotted to guide the eye.

Let us start a discussion of model predictions concerning the system-size dependence of the ratio from the string models. For simplicity of the arguments, we assume that the string formation, evolution and fragmentation is independent of $\langle W \rangle$. The yields of K^+ and π^+ mesons are proportional to the mean number of strings, and consequently, their ratio is independent of the mean number of strings, and thus it is independent of $\langle W \rangle$. The predictions of the SMASH model shown in Figure 3 approximately follow this naive expectation. The model qualitatively fails to reproduce the data.

A different system-size dependence is predicted within statistical models of nucleus–nucleus collisions. The strangeness conservation imposed on the whole system leads to a fast increase of the ratio with increasing system size to its upper limit given by the grand-canonical-ensemble approximation. The effect is referred to as canonical strangeness suppression and has been extensively studied since 1980; see, e.g., Refs. [55–57]. The PHSD model predictions shown in Figure 3 show a gradual ratio increase with $\langle W \rangle$. However, in this model, the change is likely to be also caused by smoothly increasing contributions from QGP and chiral symmetry restoration. The PHSD model describes the main properties of the data significantly better. However, it fails to reproduce the *jump* between the results for *p*+*p* and Be+Be collisions and the results for heavier nuclei at $\sqrt{s_{NN}} \approx 17$ GeV; see Figure 3 (right).

With increasing collision energy and nuclear mass number of colliding nuclei, the number of produced strings and their density is expected to increase. The idea that, at sufficiently high densities, the strings would be close enough to interact and change their properties has been developing over the last 40 years. Many approaches have been proposed, in particular, colour ropes [58], string fusion [59–63], core formation [64], string melting [65] and percolation [66,67]. A model that explicitly involves the rapid string-QGP changeover was proposed recently. It is a string collapse pictured as the black hole formation using the AdS/CFT duality [68–70]. Thus, it is natural to interpret the jump as due to a rapid changeover from strings to QGP. This changeover is called the *onset of QGP fireball*.

The gradual increase of the ratio at low collision energies (see Figure 3 (left)) is also not reproduced by the models. This can be due to the

(i) Approaching equilibrium with increasing system size and evolution time;
(ii) Weakening of the canonical strangeness suppression with increasing system size;
(iii) Increasing role of chiral symmetry restoration in dense hadronic matter.

3. Diagram of High-Energy Nuclear Collisions

Here, for the first time, we explicitly introduce a concept of the diagram of high-energy nuclear collisions and then, based on the experimental data and ideas discussed above, sketch its example version.

The diagram of high-energy nuclear collisions is defined as a plot showing domains of the dominance of different hadron-production processes in high-energy nuclear collisions. The domains are indicated in the space of laboratory-controlled parameters, the collision energy and the nuclear-mass number of colliding nuclei. For simplicity, we consider only central nucleus–nucleus collisions—collisions in which a large fraction of nucleons participated in inelastic interactions ($\langle W \rangle / \mathrm{A} \approx 1$).

To sketch the example diagram, the hadron-production processes discussed above are selected:

(i) Creation, evolution and decay of resonances;
(ii) Formation, evolution and fragmentation of strings;
(iii) Creation, evolution and hadronisation of QGP.

In addition, based on the discussion of the experimental results presented in the previous section, we assume that

(i) The Pb+Pb horn locates the resonances–QGP changeover at $\sqrt{s_{NN}} \approx 8$ GeV;
(ii) The *p*+*p* break locates the resonances–strings changeover at $\sqrt{s_{NN}} \approx 8$ GeV;
(iii) The jump between *p*+*p*/Be+Be and Ar+Sc/Pb+Pb plateaus locates the strings–QGP changeover at $\sqrt{s_{NN}} \approx 17$ GeV;
(iv) The LHC *p*+*p* data imply QGP creation in (high multiplicity) *p*+*p* interactions at sufficiently high (order of 1 TeV) energies.

The diagram of high-energy nuclear collisions following these assumptions is sketched in Figure 4.

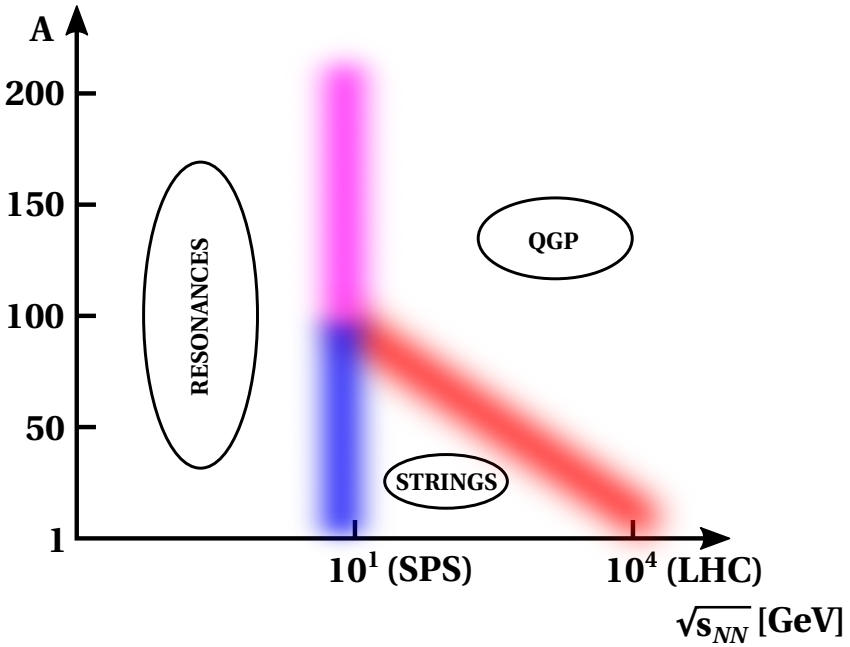

Figure 4. Schematic diagram of high-energy nuclear collisions outlined in colliding nuclei mass number, A, and collision energy, $\sqrt{s_{NN}}$ variables. Domains in which hadron production is dominated by the creation, evolution and decay of resonances, strings and quark–gluon plasma are indicated as *resonances*, *strings* and *QGP*, respectively, while thick coloured lines show the changeover regions between the domains.

Two comments are in order here.

(i) The changeover resonances–strings and resonances–QGP are located at similar collision energies (≈8 GeV/c). This suggests that the resonances–QGP changeover is driven by the resonances–strings one. At high masses of colliding nuclei, strings produced above at the resonances–strings changeover would have density exceeding the strings–QGP changeover. Thus the string domain disappears, and one observes direct resonances–QGP changeover. This locates the resonances–QGP changeover at the energy of the resonances–strings one.

(ii) It is interesting to consider other diagrams of high-energy collisions. Here, we discuss a simple example of the hadron–resonance gas diagram. Hagedorn's early papers postulated that hadrons in high-energy collisions are produced according to statistical thermodynamics [71]. Thus, following Hagedorn's postulate, the diagram would include only one production process—the statistical-thermodynamical production, with Hagedorn's temperature $T_H \approx 150$ MeV. This model is clearly in contradiction with the experimental results, as it predicts the K^+/π^+ ratio to be independent of energy and nuclear mass number of colliding nuclei. Over the years, the simple Hagedorn approach evolved into many models that are much more flexible in fitting the data; for a recent review, see Ref. [72]. In particular, it has been popular to fit mean hadron multiplicities, which include multiplicities of kaons and pions, assuming that a hadron gas in equilibrium is created at high-energy collisions. The temperature, the baryon chemical potential, and the gas volume are free parameters of the model and are fitted to the data from each reaction separately. The model cannot predict the energy and nuclear mass dependence of hadron production in this formulation. Thus, it is unsuitable for the diagram construction.

To verify the assumptions and the diagram sketched on Figure 4, further analysis of the existing data and new experimental measurements as well as the development of models is needed. Concerning modelling, there is a need for the development of dynamical models that include all three production processes. In this paper, these models are represented by PHSD [12,13] which reproduces experimental results significantly better than the SMASH

model [14,15]. The latter includes only two approaches to hadron production, resonances and strings. Still, the PHSD model misses important features of the experimental data shown in Figures 1 and 3. One must reconsider the nature of the changeover between different processes to improve predictions.

Concerning the further analysis of the existing data, one should extend the presented studies to other quantities which characterise hadron production in high-energy nuclear collisions. In particular, quantities sensitive to the collective flow of matter, radial and anisotropic should be sensitive to the production mechanisms discussed. This important study goes beyond the scope of this introductory paper.

Finally, concerning the new experimental measurements, data on light and medium mass nuclei collisions are needed—in particular, a precision system-size dependence to locate the strings–QGP changeover. Such a study was launched by NA61/SHINE at the CERN SPS, and its continuation is considered in the following years [73,74]. It would be important to perform the corresponding measurements in the full range of available energies, from the FAIR SIS-100 through NICA and SPS to CERN LHC energies. In 2024, a beam of oxygen ions is considered at the SPS and LHC in CERN [74,75], making a good start for further study. Prospects of studies with the intermediate-mass nuclear beams (e.g., Ar+Ar or Kr+Kr) at LHC energies are also vividly discussed [76].

Author Contributions: Conceptualization, E.A., M.K. and M.G.; validation, E.A., M.K. and M.G.; resources, E.A., M.K.; writing—original draft preparation, E.A., M.K. and M.G.; writing—review and editing, M.G.; visualization, M.K.; supervision, E.A., M.K. and M.G.; project administration, E.A., M.K.; All authors have read and agreed to the published version of the manuscript.

Funding: This research received no external funding.

Data Availability Statement: Data sharing not applicable.

Acknowledgments: The authors thank Mark Gorenstein and Edward Shuryak as well as members of the NA61/SHINE collaboration, in particular, Tomek Matulewicz, Andrzej Rybicki and Peter Seyboth for discussion and comments. The authors thank Elena Bratkovskaya, Viktar Kireyeu and Justin Mohs who helped in the calculation of predictions of the PHSD and SMASH models.

Conflicts of Interest: The authors declare no conflict of interest.

References

1. Shuryak, E.V. Quantum Chromodynamics and the Theory of Superdense Matter. *Phys. Rep.* **1980**, *61*, 71–158. [CrossRef]
2. Heinz, U.W.; Jacob, M. Evidence for a new state of matter: An Assessment of the results from the CERN lead beam program. *arXiv* **2000**, arXiv:nucl-th/0002042.
3. Adams, J.; et al. [STAR Collaboration] Experimental and theoretical challenges in the search for the quark gluon plasma: The STAR Collaboration's critical assessment of the evidence from RHIC collisions. *Nucl. Phys. A* **2005**, *757*, 102–183. [CrossRef]
4. Gazdzicki, M.; Gorenstein, M.; Seyboth, P. Onset of deconfinement in nucleus–nucleus collisions: Review for pedestrians and experts. *Acta Phys. Polon. B* **2011**, *42*, 307–351. [CrossRef]
5. Gazdzicki, M.; Gorenstein, M.; Seyboth, P. Brief history of the search for critical structures in heavy-ion collisions. *Acta Phys. Polon. B* **2020**, *51*, 1033. [CrossRef]
6. Florkowski, W. *Phenomenology of Ultra-Relativistic Heavy-Ion Collisions*; World Scientific: Singapore, 2010; Volume 3. [CrossRef]
7. Karsch, F. Lattice QCD at high temperature and density. *Lect. Notes Phys.* **2002**, *583*, 209–249.
8. Werner, K. Strings, pomerons, and the venus model of hadronic interactions at ultrarelativistic energies. *Phys. Rep.* **1993**, *232*, 87–299. [CrossRef]
9. Bleicher, M.; Zabrodin, E.; Spieles, C.; Bass, S.A.; Ernst, C.; Soff, S.; Bravina, L.; Belkacem, M.; Weber, H.; Stöcker, H.; Greiner, W., Relativistic hadron hadron collisions in the ultrarelativistic quantum molecular dynamics model. *J. Phys. G* **1999**, *25*, 1859–1896. [CrossRef]
10. Rafelski, J.; Muller, B. Strangeness Production in the Quark-Gluon Plasma. *Phys. Rev. Lett.* **1982**, *48*, 1066. Erratum: *Phys. Rev. Lett.* **1986**, *56*, 2334. [CrossRef]
11. Gazdzicki, M.; Gorenstein, M.I. On the early stage of nucleus–nucleus collisions. *Acta Phys. Polon. B* **1999**, *30*, 2705.
12. Cassing, W.; Bratkovskaya, E.L. Parton transport and hadronization from the dynamical quasiparticle point of view. *Phys. Rev. C* **2008**, *78*, 034919. [CrossRef]
13. Cassing, W.; Bratkovskaya, E.L. Parton-Hadron-String Dynamics: An off-shell transport approach for relativistic energies. *Nucl. Phys. A* **2009**, *831*, 215–242. [CrossRef]

14. Weil, J.; Steinberg, V.; Staudenmaier, J.; Pang, L.G.; Oliinychenko, D.; Mohs, J.; Kretz, M.; Kehrenberg, T.; Goldschmidt, A.; Bäuchle, B.; et al. Particle production and equilibrium properties within a new hadron transport approach for heavy-ion collisions. *Phys. Rev. C* **2016**, *94*, 054905. [CrossRef]
15. Mohs, J.; Ryu, S.; Elfner, H. Particle Production via Strings and Baryon Stopping within a Hadronic Transport Approach. *J. Phys. G* **2020**, *47*, 065101. [CrossRef]
16. Alt, C.; et al. [NA49 Collaboration] Pion and kaon production in central Pb + Pb collisions at 20-A and 30-A-GeV: Evidence for the onset of deconfinement. *Phys. Rev. C* **2008**, *77*, 024903. [CrossRef]
17. Afanasiev, S.V.; et al. [NA49 Collaboration] Energy dependence of pion and kaon production in central Pb + Pb collisions. *Phys. Rev. C* **2002**, *66*, 054902. [CrossRef]
18. Abelev, B.; et al. [ALICE Collaboration] Centrality dependence of π, k, and p production in Pb-Pb collisions at $\sqrt{s_{NN}} = 2.76$ TeV. *Phys. Rev. C* **2013**, *88*, 044910. [CrossRef]
19. Acharya, S.; et al. [ALICE Collaboration] Production of charged pions, kaons, and (anti-)protons in Pb-Pb and inelastic pp collisions at $\sqrt{s_{NN}}$ = 5.02 TeV. *Phys. Rev. C* **2020**, *101*, 044907. [CrossRef]
20. Ahle, L.; et al. [E866 Collaboration] Excitation function of K^+ and p^+ production in Au + Au reactions at 2/A-GeV to 10/A-GeV. *Phys. Lett. B* **2000**, *476*, 1–8. [CrossRef]
21. Klay, J.L.; et al. [E895 Collaboration] Charged pion production in 2 to 8 AGeV central Au+Au collisions. *Phys. Rev. C* **2003**, *68*, 054905. [CrossRef]
22. Adamczyk, L.; et al. [STAR Collaboration] Bulk Properties of the Medium Produced in Relativistic Heavy-Ion Collisions from the Beam Energy Scan Program. *Phys. Rev. C* **2017**, *96*, 044904. [CrossRef]
23. Adam, J.; et al. [STAR Collaboration] Bulk properties of the system formed in $Au + Au$ collisions at $\sqrt{s_{\rm NN}}$ =14.5 GeV at the BNL STAR detector. *Phys. Rev. C* **2020**, *101*, 024905. [CrossRef]
24. Abelev, B.I.; et al. [STAR Collaboration] Systematic Measurements of Identified Particle Spectra in pp, d^+ Au and Au+Au Collisions from STAR. *Phys. Rev. C* **2009**, *79*, 034909. [CrossRef]
25. Adamczewski-Musch, J.; et al. [HADES Collaboration] Deep sub-threshold ϕ production in au+au collisions. *Physics Letters B* **2018**, *778*, 403–407. [CrossRef]
26. Adamczewski-Musch, J.; et al. [HADES Collaboration] Charged-pion production in Au+Au collisions at $\sqrt{s_{NN}}$=2.4 GeV: HADES Collaboration. *Eur. Phys. J. A* **2020**, *56*, 259.
27. Aduszkiewicz, A.; et al. [NA61/SHINE Collaboration] Measurements of $\pi^{\pm}$, $K^{\pm}$, p and $\overline{p}$ spectra in proton–proton interactions at 20, 31, 40, 80 and 158 GeV/c with the NA61/SHINE spectrometer at the CERN SPS. *Eur. Phys. J. C* **2017**, *77*, 671. [CrossRef]
28. Adare, A.; et al. [PHENIX Collaboration] Identified charged hadron production in $p + p$ collisions at $\sqrt{s} = 200$ and 62.4 GeV. *Phys. Rev. C* **2011**, *83*, 064903. [CrossRef]
29. Aamodt, K.; et al. [ALICE Collaboration] Production of pions, kaons and protons in pp collisions at $\sqrt{s} = 900$ GeV with ALICE at the LHC. *Eur. Phys. J. C* **2011**, *71*, 1655. [CrossRef]
30. Adam, J.; et al. [ALICE Collaboration] Measurement of pion, kaon and proton production in proton–proton collisions at $\sqrt{s} = 7$ TeV. *Eur. Phys. J. C* **2015**, *75*, 226. [CrossRef]
31. Acharya, S.; et al. [ALICE Collaboration] Production of light-flavor hadrons in pp collisions at $\sqrt{s} = 7$ and $\sqrt{s} = 13$ TeV. *Eur. Phys. J. C* **2021**, *81*, 256. [CrossRef]
32. Veneziano, G. Construction of a crossing—Symmetric, Regge behaved amplitude for linearly rising trajectories. *Nuovo Cim. A* **1968**, *57*, 190–197. [CrossRef]
33. Aduszkiewicz, A.; et al. [NA61/SHINE Collaboration] Proton-Proton Interactions and Onset of Deconfinement. *Phys. Rev. C* **2020**, *102*, 011901. [CrossRef]
34. Andersson, B.; Gustafson, G.; Ingelman, G.; Sjostrand, T. Parton Fragmentation and String Dynamics. *Phys. Rep. B* **1983**, *97*, 31–145. [CrossRef]
35. Kaidalov, A.B.; Ter-Martirosian, K.A. Pomeron as Quark-Gluon Strings and Multiple Hadron Production at SPS Collider Energies. *Phys. Lett. B* **1982**, *117*, 247–251. [CrossRef]
36. Capella, A.; Sukhatme, U.; Tan, C.-I., Tran Thanh Van, J. Dual parton model. *Phys. Rep.* **1994**, *236*, 225–329. [CrossRef]
37. Bass, S.A.; Belkacem, M.; Bleicher, M.; Brandstetter, M.; Bravina, L.; Ernst, C.; Gerland, L.; Hofmann, M.; Hofmann, S.; Konopka, J.; et al. Microscopic models for ultrarelativistic heavy ion collisions. *Prog. Part. Nucl. Phys.* **1998**, *41*, 255–369. [CrossRef]
38. Vovchenko, V.Y.; Anchishkin, D.V.; Gorenstein, M.I. Mean transverse mass of hadrons in proton–proton reactions. *Nucl. Phys. A* **2015**, *936*, 1–5. [CrossRef]
39. Adam, J.; et al. [ALICE Collaboration] Enhanced production of multi-strange hadrons in high-multiplicity proton–proton collisions. *Nat. Phys.* **2017**, *13*, 535–539. [CrossRef]
40. Chatrchyan, S.; et al. [CMS Collaboration] Observation of long-range near-side angular correlations in proton-lead collisions at the LHC. *Phys. Lett.* **2013**, *B718*, 795–814.
41. Khachatryan, V.; et al. [CMS Collaboration] Evidence for collectivity in pp collisions at the LHC. *Phys. Lett.* **2017**, *B765*, 193–220.
42. Nagle, J.L.; Zajc, W.A. Small System Collectivity in Relativistic Hadronic and Nuclear Collisions. *Ann. Rev. Nucl. Part. Sci.* **2018**, *68*, 211–235. [CrossRef]
43. Bozek, P.; Broniowski, W. Theory of pp/pA/small systems. In Proceedings of the Fourth Annual Large Hadron Collider Physics, Lund, Sweden, 13–18 June 2016.

44. Abgrall, N.; et al. [NA61/SHINE Collaboration] NA61/SHINE facility at the CERN SPS: Beams and detector system. *J. Instrum.* **2014**, *9*, P06005. [CrossRef]
45. Gazdzicki, M.; Fodor, Z.; Vesztergombi, G. *Study of Hadron Production in Hadron-Nucleus and Nucleus-Nucleus Collisions at the CERN SPS*; Technical Report; CERN: Geneva, Switzerland, 2006.
46. Acharya, A.; et al. [NA61/SHINE Collaboration]Measurements of $\pi^{\pm}$, $K^{\pm}$, p and $\overline{p}$ spectra in ^{7}Be+^{9}Be collisions at beam momenta from 19A to 150A GeV/c with the NA61/SHINE spectrometer at the CERN SPS. *Eur. Phys. J. C* **2021**, *81*, 73. [CrossRef]
47. Alt, C.; et al. [NA49 Collaboration] System-size dependence of strangeness production in nucleus–nucleus collisions at s(NN)**(1/2) = 17.3-GeV. *Phys. Rev. Lett.* **2005**, *94*, 052301. [CrossRef] [PubMed]
48. Anticic, T.; et al. [NA49 Collaboration] System-size and centrality dependence of charged kaon and pion production in nucleus–nucleus collisions at 40A GeV and158A GeV beam energy. *Phys. Rev. C* **2012**, *86*, 054903. [CrossRef]
49. Abbott, T.; Akiba, Y.; Beavis, D.; Bloomer, M.A.; Bond, P. D.; Chasman, C.; Chen, Z.; Chu, Y.Y.; Cole, B.A.; Costales, J.B.; et al. Charged hadron distributions in central and peripheral Si + A collisions at 14.6-A/GeV/c. *Phys. Rev. C* **1994**, *50*, 1024–1047. [CrossRef]
50. Lewicki, M.P.; Turko, L. NA61/SHINE shining more light on the onset of deconfinement. *arXiv* **2020**, arXiv:2002.00631
51. Acharya, A.; et al. [NA61/SHINE Collaboration] Spectra and mean multiplicities of π^{-} in central^{40}Ar+^{45}Sc collisions at 13A, 19A, 30A, 40A, 75A and 150A GeV/c beam momenta measured by the NA61/SHINE spectrometer at the CERN SPS. *Eur. Phys. J. C* **2021**, *81*, 397. [CrossRef]
52. Best, D.; et al. [FOPI Collaboration] K+ production in the reaction Ni-58 + Ni-58 at incident energies from 1-A/GeV to 2-A/GeV. *Nucl. Phys. A* **1997**, *625*, 307–324. [CrossRef]
53. Pelte, D.; et al. [FOPI Collaboration] Charged pions from Ni on Ni collisions between 1-A/Gev and 2-A/GeV. *Z. Phys. A* **1997**, *359*, 55–65. [CrossRef]
54. Acharya, S.; et al. [ALICE Collaboration] Production of pions, kaons, (anti-)protons and ϕ mesons in Xe–Xe collisions at $\sqrt{s_{\mathrm{NN}}}$ = 5.44 TeV. *Eur. Phys. J. C* **2021**, *81*, 584. [CrossRef]
55. Rafelski, J.; Danos, M. The Importance of the Reaction Volume in Hadronic Collisions. *Phys. Lett. B* **1980**, *97*, 279–282. [CrossRef]
56. Redlich, K.; Turko, L. Phase Transitions in the Statistical Bootstrap Model with an Internal Symmetry. *Z. Phys. C* **1980**, *5*, 201. [CrossRef]
57. Becattini, F.; Ferroni, L. Statistical hadronization and hadronic microcanonical ensemble. 1.. *Eur. Phys. J. C* **2004**, *35*, 243–258. [CrossRef]
58. Biro, T.S.; Nielsen, H.B.; Knoll, J. Color Rope Model for Extreme Relativistic Heavy Ion Collisions. *Nucl. Phys. B* **1984**, *245*, 449–468. [CrossRef]
59. Braun, M.; Pajares, C. A Probabilistic model of interacting strings. *Nucl. Phys. B* **1993**, *390*, 542–558. [CrossRef]
60. Braun, M.A.; Pajares, C. Particle production in nuclear collisions and string interactions. *Phys. Lett. B* **1992**, *287*, 154–158. [CrossRef]
61. Braun, M.A.; Pajares, C.; Vechernin, V.V. Ridge from Strings. *Eur. Phys. J. A* **2015**, *51*, 44. [CrossRef]
62. Braun, M.A.; de Deus, J.D.; Hirsch, A.S.; Pajares, C.; Scharenberg, R.P.; Srivastava, B.K. De-Confinement and Clustering of Color Sources in Nuclear Collisions. *Phys. Rep.* **2015**, *599*, 1–50. [CrossRef]
63. Ramírez, J.E.; Díaz, B.; Pajares, C. Interacting color strings as the origin of the liquid behavior of the quark–gluon plasma. *Phys. Rev. D* **2021**, *103*, 094029. [CrossRef]
64. Werner, K. Core-corona separation in ultra-relativistic heavy ion collisions. *Phys. Rev. Lett.* **2007**, *98*, 152301. [CrossRef] [PubMed]
65. Lin, Z.-W.; Ko, C.M.; Li, B.-A.; Zhang, B.; Pal, S. A Multi-phase transport model for relativistic heavy ion collisions. *Phys. Rev. C* **2005**, *72*, 064901. [CrossRef]
66. Digal, S.; Fortunato, S.; Satz, H. Predictions for J/psi suppression by parton percolation. *Eur. Phys. J. C* **2004**, *32*, 547–553. [CrossRef]
67. Hohne, C.; Puhlhofer, F.; Stock, R. System-size dependence of strangeness production in high-energy a+a collisions and percolation of strings. *Phys. Lett. B* **2006**, *640*, 96–100. [CrossRef]
68. Kalaydzhyan, T.; Shuryak, E. Collective interaction of QCD strings and early stages of high multiplicity pA collisions. *Phys. Rev. C* **2014**, *90*, 014901. [CrossRef]
69. Kalaydzhyan, T.; Shuryak, E. Self-interacting QCD strings and string balls. *Phys. Rev. D* **2014**, *90*, 025031. [CrossRef]
70. Iatrakis, I.; Ramamurti, A.; Shuryak, E. Collective String Interactions in AdS/QCD and High-Multiplicity pA Collisions. *Phys. Rev. D* **2015**, *92*, 014011. [CrossRef]
71. Hagedorn, R. Statistical thermodynamics of strong interactions at high-energies. *Nuovo Cim. Suppl.* **1965**, *3*, 147–186.
72. Andronic, A.; Braun-Munzinger, P.; Redlich, K.; Stachel, J. Decoding the phase structure of QCD via particle production at high energy. *Nature* **2018**, *561*, 321–330. [CrossRef]
73. Fields, L.; Podlaski, P.; et al. [NA61/SHINE Collaboration] *Report from the NA61/SHINE Experiment at the CERN SPS*; Technical Report; CERN: Geneva, Switzerland, 2020.
74. Gazdzicki, M.; et al. [NA61/SHINE Collaboration] *Addendum to the NA61/SHINE Proposal: Request for Oxygen Beam in Run 3*; Technical Report; CERN: Geneva, Switzerland, 2022.

75. Brewer, J.; Mazeliauskas, A.; van der Schee, W. Opportunities of OO and *p*O collisions at the LHC. *arXiv* **2021**, arXiv:2103.01939.
76. Citron, Z.; Dainese, A.; Grosse-Oetringhaus, J.F.; Jowett, J.M.; Lee, Y.-J.; Wiedemann, U.A.; Winn, M.; Andronic, A.; Bellini, F.; Bruna, E.; et al. Report from Working Group 5: Future physics opportunities for high-density QCD at the LHC with heavy-ion and proton beams. *CERN Yellow Rep. Monogr.* **2019**, *7*, 1159–1410.